

Improving the dE/dx calibration of the STAR TPC for the high- p_T hadron identification

Yichun Xu ^{a,b,*}, Olga Barannikova ^h, Hans Bichsel ^c,
Xin Dong ^{a,d}, Patricia Fachini ^b, Yuri Fisyak ^b,
Adam Kocoloski ^e, Bedanga Mohanty ^f, Pawan Netrakanti ^g,
Lijuan Ruan ^b, Maria Cristina Suarez ^h, Zebo Tang ^{a,b},
Gene van Buren ^b, Zhangbu Xu ^{a,b}

^a*Department of Modern Physics, University of Science and Technology of China,
Hefei, Anhui, China, 230026*

^b*Department of Physics, Brookhaven National Laboratory, Upton, NY 11973, USA*

^c*Nuclear Physics Laboratory, University of Washington, Box 354290, Seattle, WA
98195-4290, USA*

^d*Lawrence Berkeley National Laboratory, 1 Cyclotron Road, Berkeley, CA 94720,
USA*

^e*Massachusetts Institute of Technology, 77 Massachusetts Avenue, Cambridge, MA
02139-4307, USA*

^f*Variable Energy Cyclotron Centre, Kolkata 700064, India*

^g*Purdue University, West Lafayette, Indiana 47907, USA*

^h*University of Illinois at Chicago, Department of Physics 845 W. Taylor St., M/C
273 Chicago, IL 60607-7059, USA*

Abstract

We derive a method to improve particle identification (PID) at high transverse momentum (p_T) using the relativistic rise of the ionization energy loss (dE/dx) when charged particles traverse the Time Projection Chamber (TPC) at STAR. Electrons triggered and identified by the Barrel Electro-Magnetic Calorimeter (BEMC), pure protons(anti-protons) and pions from Λ ($\bar{\Lambda}$), and K_S^0 decays are used to obtain the dE/dx value and its width at given $\beta\gamma = p/m$. We found that the deviation of the dE/dx from the Bichsel function can be up to 0.4σ ($\sim 3\%$) in p+p collisions at $\sqrt{s_{NN}} = 200$ GeV taken and subsequently calibrated in year 2005. The deviation is approximately a function of $\beta\gamma$ independent of particle species and can be described with the function $f(x) = A + \frac{B}{C+x^2}$. The deviations obtained with this method are used in the data sample from p+p collision for physics analysis of identified hadron spectra and their correlations up to transverse momentum of 15 GeV/c. The ratio of e^-/e^+ (dominantly from γ -conversion) is also used to correct for the residual momentum distortion in the STAR TPC.

Key words: TPC, ionization energy loss, relativistic rise

PACS: 29.40.Cs, 29.85.Fj

1 Introduction

Identified hadron (π^\pm , K^\pm , $p(\bar{p})$) spectra at high p_T in p+p collisions provide a good test of perturbative quantum chromodynamics (pQCD) [1] and a baseline for studying color charge effect of parton energy loss in heavy ion collisions [2,3]. Hadron identification at high p_T was achieved with the ionization energy loss (dE/dx) at the relativistic rise using the STAR Time Projection Chamber (TPC). The dE/dx for a given charged-particle track is calculated using a well-

* +1-631-344-7635

Email address: xuychun@mail.ustc.edu.cn (Yichun Xu).

8 known method called "truncated mean". The dE/dx values of hits associated
9 with the track have a typical Landau tail. The hits with the top 30% of high
10 dE/dx values are discarded and an average of dE/dx value from the rest
11 of the hits is derived for that track [9]. The dE/dx for a given particle at
12 low momentum decreases with increasing momentum to reach a minimum
13 ionization, then increases due to the relativistic rise. For a minimum ionizing
14 particle (MIP) the dE/dx resolution in the STAR TPC is 6-8% for a track
15 with the maximum of 45 sampled dE/dx points. The pions are well separated
16 from the rest of the particles (e, K, p) at p_T of 0.3 to 0.6 GeV/ c . This clear
17 separation has been used to calibrate the TPC dE/dx without other means of
18 identification. It provides the fixed points for extrapolating the dE/dx function
19 to higher momentum. In the thin material (TPC gas) the Bichsel function has
20 proved to be a very good approximation for the dE/dx curves and has been
21 adopted by STAR as a standard method of predicting the dE/dx value for
22 charged hadrons in all momentum ranges [4].

23 The Landau function is an approximation which does not include features
24 related to atomic structure. With the Bichsel function [4], a decrease of the
25 relativistic rise of dE/dx with increasing segment length x is seen and param-
26 eterized empirically. This effect, gas multiplication gains and noise of TPC
27 electronics and pileup in high luminosity environment may make the dE/dx
28 deviate from the Bichsel function. In the relativistic rise region, the dE/dx sep-
29 arations among π^\pm, K^\pm and $p(\bar{p})$ are about $1-3\sigma$ with the dE/dx amplitude of
30 pions the highest and that of protons the lowest. Pions are the dominant par-
31 ticle species for inclusive and jet hadrons, and they shadow kaons and protons
32 in the dE/dx distribution. In a given momentum slice, clear peak separations
33 of these three hadrons are not possible. This results in large systematic er-

34 rors due to the uncertainty of the dE/dx positions. From the minimum-bias
35 triggered p+p collisions in the year 2003, the $p(\bar{p})$ spectra were measured to
36 $p_T \lesssim 7$ GeV/ c with significant systematic errors due to the uncertainties in
37 determining the mean dE/dx position for proton and kaon [3]. Knowledge of
38 the precise dE/dx positions for those hadrons is important to understand the
39 efficiencies of PID selection and to reduce the systematic uncertainty in iden-
40 tified hadron yields. In order to improve the particle identification at high p_T ,
41 we develop a method to locate the dE/dx positions for different hadrons with
42 good precision.

43 The p+p collision events with enhanced high- p_T charged particles used in this
44 analysis were obtained from online jet trigger by the BEMC with $0 < \eta <$
45 1 in the year 2005, and full azimuthal coverage. $\Lambda \rightarrow p + \pi^-$ ($\bar{\Lambda} \rightarrow \bar{p} + \pi^+$)
46 and $K_S^0 \rightarrow \pi^+\pi^-$ are reconstructed by their decay topology to identify their
47 decay daughters – charged pions and protons. The identified electrons, pions
48 and protons provide the necessary distinct dE/dx positions and widths as
49 function of $\beta\gamma$. The deviation from the prediction of the Bichsel function was
50 used to correct for the dE/dx fit when extracting pion and proton yields from
51 the charged hadrons in an inclusive hadron distribution or in a jet. The same
52 method can be applied to p+p, d+Au and A+A collisions in STAR.

53 Physics goals of the STAR Experiment at RHIC in recent (and future) years [5]
54 drive the need to operate the STAR TPC at ever higher luminosity, and in-
55 crease the ionization density in the TPC gas [6]. The resulting ionic space
56 charge and grid leakage introduce field distortions in the detector, which sys-
57 tematically shift the reconstructed momentum of positive and negative parti-
58 cles in opposite directions. The effect is expected to grow as a function of
59 p_T . STAR has developed a method for correcting the track reconstruction due

60 to space charge distortion. Performance of the corrections can be assessed by
61 examining the distribution of signed DCA (Distance of Closest Approach of
62 a primary track to the collision vertex) as a function of luminosity. In this
63 paper, we use electrons and positrons dominantly from gamma conversion to
64 check and correct for potential residuals from the distortion. We expect e^-/e^+
65 to be unity independent of p_T since $\gamma \rightarrow e^- + e^+$ and a significant fraction
66 of leptons from heavy-flavor decays are also expected to be close to unity [7].
67 The high-statistics data set from BEMC trigger is ideal for such a study.

68 **2 Experimental Setup and Data Analysis**

69 *2.1 Detectors and Datasets*

70 The Solenoidal Tracker at RHIC (STAR) [8] is a powerful detector with a large
71 and uniform acceptance capable of tracking charged particle and providing
72 particle identification (PID). Its main tracking detector – TPC [9] covers full
73 azimuthal angle ($\Delta\phi = 2\pi$) and $-1.3 < \eta < 1.3$ in pseudo-rapidity, and
74 provides identification of the charged hadrons by measuring momentum and
75 dE/dx separation of the charged particles. The STAR TPC has 45 rows of
76 pads with the first pad row at a radius of 60 cm and last at 180 cm, providing
77 a maximum of 45 sampled dE/dx points with 78 cm track length in a P10
78 gas (90% Argon and 10% CH_4) while Track lengths of up to 110 cm are
79 possible. In order to obtain the dE/dx position of protons at the relativistic
80 rise range, protons (anti-protons) are selected from Λ ($\bar{\Lambda}$) decays. Similarly,
81 decay pions from K_S^0 can be used to get dE/dx and dE/dx positions of pions
82 for $0.2 < p_T < 3$ GeV/c. The precise track geometry allows the particle

83 trajectories to be extrapolated to form a $V0$ away from the collision vertex [10].
 84 This provides dE/dx information from samples of pure protons and charged
 85 pions.

86 In addition, the sub-detector BEMC [11] is also used to enhance electron and
 87 positron yields and to confirm their identification. This study used about 16.7
 88 million p+p collision events recorded through online High Tower (HT) and
 89 Jet Patch (JP) triggers in the BEMC. The HT trigger condition required the
 90 energy of a single calorimeter tower ($\Delta\eta \times \Delta\phi = 0.05 \times 0.05$) to be at least
 91 2.6 (HT1) or 3.6 (HT2) GeV, and JP trigger required the total energy of one
 92 patch of towers ($\Delta\eta \times \Delta\phi = 1.0 \times 1.0$) to exceed 4.5 (JP1) or 6.5 (JP2)
 93 GeV [12].

94 2.2 dE/dx distribution in the TPC at high p_T

95 To formulate the dE/dx ¹ distribution and its associated Bichsel function for
 96 PID, we need to define a few terms. The normalized dE/dx is defined as
 97 $n\sigma_X^Y = \log[(dE/dx)_Y/B_X]/\sigma_X$, where X,Y can represent π^\pm , K^\pm , $p(\bar{p})$ or e^\pm ;
 98 B_X is the expected mean dE/dx of particle X; and σ_X is the $\ln(dE/dx/B_X)$
 99 resolution of the TPC [13,14,15]. All the quantities are calculated in a track-
 100 by-track basis. Fig. 1 shows $n\sigma_\pi$ distribution of all the charged particles for
 101 $3.75 < p_T < 4.0$ GeV/ c and $8.0 < p_T < 10.0$ GeV/ c at $|\eta| < 0.5$. A sum of eight
 102 Gaussian functions is used to fit this distribution with thirteen parameters
 103 in order to obtain the identified hadron yields. Each Gaussian describes one
 104 dE/dx distribution for a charged particle species. The thirteen parameters are
 105 peak positions relative to pion peak ($n\sigma_\pi^\pi$, $n\sigma_\pi^K - n\sigma_\pi^\pi$, $n\sigma_\pi^p - n\sigma_\pi^\pi$, $n\sigma_\pi^e - n\sigma_\pi^\pi$), eight

¹ dE/dx is used to represent the “track descriptor” C defined on p.170 of [4]

106 yields for the charged particles and one common Gaussian width. With ideal
 107 calibration, $n\sigma_\pi^\pi$ should be a normal Gaussian distribution centered at zero and
 108 with a width of unity. The normality of Gaussians depends on the precision of
 109 σ_X in a track-by-track basis. As presented in Ref. [4] (section 6.2 and Fig. 21,
 110 22, and 23), the σ_X depends on the track length (t) in the dE/dx sample. An
 111 empirical parameterization yields $\sigma_\pi = \sigma_0/t^s$ where $0.45 < s < 0.55$ [4]. Fig. 2
 112 shows the dE/dx resolution as a function of track length for this specific run
 113 in p+p collisions at center of mass energy of 200 GeV in year 2005. The red
 114 solid curve is a power-law fit with $s = 0.52$ in the range of $40 < t < 80$ cm,
 115 where the majority of the tracks come from. A polynomial function was also
 116 performed at larger range and was shown as dashed line.

117 Fig. 1 shows that the pion dE/dx position is different from the Bichsel func-
 118 tion. This means that the dE/dx calibration is not perfect and it also implies
 119 that dE/dx position of other particles relative to that of the pions may be off
 120 from their expected values. In order to improve the particle identification and
 121 reduce the systematic uncertainty in identified particle yields obtained from
 122 dE/dx [2,3], we study in details the precise dE/dx positions of all charged par-
 123 ticles using the enhanced electron by the BEMC, pure proton decayed from
 124 from Λ and pion decayed from K_S^0 in the TPC. Once all the dE/dx positions
 125 and widths for all the charged hadrons are obtained by other means, we will be
 126 able to constrain better the Gaussian fits, and understand the efficiency and
 127 contamination better in the case of PID selections for other physics analysis.

129 Although electron dE/dx is relatively far away from those of the other charged
130 particles, the electron yields are orders of magnitudes lower than the yields
131 for pions. In order to identify the electron and obtain its dE/dx position, a
132 dataset with a special trigger based on the energy deposited in the BEMC
133 tower is used to enhance the yield of electrons relative to other particles. Ad-
134 ditional hadron rejection is achieved from the shower shape and position from
135 a Shower Maximum Detector (SMD) [11], which is located at ~ 5.6 radiation
136 lengths depth in the BEMC. A unique feature of the SMD is its double layer
137 design which makes it possible to reconstruct the shower as two-dimensional
138 image, so that it can provide fine spatial resolution in ϕ and η directions and
139 reject hadrons according to the different shower shape between hadrons and
140 electrons. We require p/E to be $0.3 < p/E < 1.5$ where p is track momentum in
141 the TPC and E is the energy of the BEMC tower, and the shower hits of the
142 SMD in η and ϕ direction to be $n_\eta \geq 2$ and ϕ direction $n_\phi \geq 2$, respectively.
143 The different positions between hit and track projection in ϕ and z directions
144 are restricted to be $|\phi_{dist}| \leq 0.01$ rad and $|z_{dist}| \leq 2$ cm [11]. The $n\sigma_\pi^h$ dis-
145 tribution for track after these cuts are shown on Fig. 3 for $3.75 < p_T < 4.0$
146 GeV/ c and at much higher p_T range. With about $1.5\text{-}3\sigma$ separation between
147 electron (positron) and other hadrons, electron position and yields could be
148 obtained from the eight-Gaussian function as above. From the same fit, we
149 can also obtain the dE/dx positions for pions, which are labeled as “pion with
150 EMC” for later use.

151 To correct for and to assess the systematic errors due to the residual mo-
152 mentum distortion, we use e^-/e^+ ratio as a function of p_T . Fig. 4 shows the

153 ratio as a function of p_T obtained from the BEMC triggered data described as
 154 above. If the electron and positron yields are a modified power-law function
 155 ($f(p_T) \propto (p_0 + p_T)^{-n}$) without any distortion, the distortion due to space
 156 charge in the TPC shifts all negatively charged tracks from p_T value to a
 157 higher $p_T + A \times p_T^2$ while it shifts all positively charged tracks from p_T value
 158 to a lower $p_T - A \times p_T^2$ [6]. The correction form is according to the effect of
 159 sagitta displacement due to space charge on momentum distortion [16]. Data
 160 points are fitted by the following function $f(p_T) = \left(\frac{2.67+p_T+A*p_T^2}{2.67+p_T-A*p_T^2}\right)^{11.4}$, where
 161 $A * p_T^2$ means Δp_T affected by charge distortion, and $p_0 = 2.67$ and $n = 11.4$
 162 are parameters obtained from the inclusive electron spectra [7]. The p_T depen-
 163 dence of ratios indicates that the momenta of the charged particles obtained
 164 from the TPC tracking still systematically shifted away from their true value
 165 due to the space charge distortion. We note that the obtained distortion char-
 166 acterized by parameter A is only about 2σ from zero and this results in about
 167 1.3% momentum shift for a single particle track at $p_T = 15$ GeV/ c .

168 2.4 Proton and pion from V0 reconstructed in the TPC

169 In order to obtain the dE/dx position of proton ($n\sigma_\pi^p$) for $\beta\gamma > 4$, protons
 170 (anti-protons) are selected from Λ ($\bar{\Lambda}$) through $\Lambda \rightarrow p + \pi^-$ ($\bar{\Lambda} \rightarrow \bar{p} + \pi^+$)
 171 decays, because it is difficult to get dE/dx position of proton by $h^+ - h^-$ [13]
 172 with this data sample due to low statistics and small difference of yields of
 173 proton and anti-proton. At the same time, pions decayed from K_S^0 through
 174 $K_S^0 \rightarrow \pi^+ + \pi^-$ decay can be used to get dE/dx and dE/dx positions of pion
 175 ($n\sigma_\pi^\pi$) at $0.2 < p_T < 3$ GeV/ c . First, K_S^0 and Λ are selected by topological cuts
 176 on a secondary vertex [10] according to long decay length of K_S^0 ($c\tau=2.6$ cm)

177 and Λ ($c\tau=7.89$ cm). Fig. 5 shows the invariant mass distribution for K_S^0 (top
 178 panel) and Λ (bottom panel). Pure K_S^0 and Λ ($\bar{\Lambda}$) are selected via their in-
 179 variant mass cuts, $0.485 < M(K_S^0) < 0.505$ GeV/ c^2 and $1.112 < M(\Lambda) < 1.12$
 180 GeV/ c^2 , and their daughter particles ($\pi, p(\bar{p})$) with high purity are obtained
 181 to derive $n\sigma_\pi^p$ and $n\sigma_\pi^\pi$. Fig. 6 shows $n\sigma_\pi^h$ distribution of pions decayed from
 182 K_S^0 (upper panel) fitted by a Gaussian function and protons decayed from Λ
 183 (lower panel) fitted by a 2-Gaussian function. The protons from Λ decay have
 184 higher background (signal-to-background ratio = 9:1) and a second Gaussian
 185 representing the pion contamination is necessary. Meanwhile, the p_T depen-
 186 dence of the dE/dx width for protons and pions from the fits are shown in
 187 Fig. 7, which also shows dE/dx width for electron. The width is consistently
 188 smaller than unity (0.868 ± 0.004). This means that the dE/dx resolution is
 189 about 13% better than the prediction and the separations among particles
 190 are better than what we expected. This may be due to the run to run vari-
 191 ation (luminosity, beam background, etc.), and our calibration only sampled
 192 a small fraction of data ($\sim 5\%$). The open triangles in Fig. 7 shows the sole
 193 effect of the smearing of the dE/dx peak positions between proton and pion
 194 due to the variation of the track quality (σ_π^p). This effect ($< 0.2\sigma$), compared
 195 quadratically to the dE/dx width, contributes $< 4\%$ to the final dE/dx width.

196 2.5 dE/dx deviation vs $\beta\gamma$

197 With identified pion, proton and electron mentioned above, the experimental
 198 results on the deviation of the normalized dE/dx ($n\sigma_\pi^h$) relative to the Bichsel
 199 theoretical values, as a function of $\beta\gamma$ are shown on Fig. 8. Since there is
 200 almost no particle species dependence of dE/dx , we can describe it with a

201 function of $f(x) = A + \frac{B}{C+x^2}$. The fit parameters are listed in Tab. 1. With
 202 this, we can determine the dE/dx positions and widths of any given charged
 203 particles to better than $< 0.1\sigma$ or $< 1\%$.

204 There are two ways to correct for this effect in the data. One can attempt
 205 to understand the origin of this deviation and correct for the effect at the
 206 hit level (the amplitudes of the ionization signal in each pad and row). This
 207 requires re-processing of the hits and reconstructing tracks from scratch. In
 208 order to take advantage of the existing compressed dataset with tracking in-
 209 formation only, we apply the corrections to the dE/dx Gaussian function for
 210 each particle species without modifying the dE/dx itself. This empirical after-
 211 burner is applied in each p_T and rapidity bin to directly extract particle yields
 212 required by the physics analyses. Fig. 9 shows p_T/mass dependence of the
 213 normalized dE/dx deviation, which is fitted by the same function as for the
 214 case of p/mass . The parameters from the function are shown in Tab. 1. With
 215 the corrected deviation, differences of dE/dx between pion and other charged
 216 particles ($n\sigma_\pi^K - n\sigma_\pi^\pi$, $n\sigma_\pi^p - n\sigma_\pi^\pi$ and $n\sigma_\pi^e - n\sigma_\pi^\pi$) are calculated and compared
 217 with theoretical values and shown in Fig. 10. Clear offsets are depicted in
 218 Fig. 10.

219 **3 Summary**

220 The dE/dx positions and widths of charged particles have been precisely de-
 221 termined using BEMC triggered events with enhanced electron content and
 222 pure samples of pions and protons from K0s and Lambda decays respectively.
 223 Their deviations relative to theoretical values versus $\beta\gamma$ and p_T/mass are de-
 224 scribed by the function $f(x) = A + \frac{B}{C+x^2}$ very well. With this method, dE/dx

225 positions of charged particles are re-calibrated to be better than 0.1σ . The
226 particle identification of charged hadrons is thus improved, and the uncer-
227 tainty is reduced significantly. These are important steps toward fulfilling the
228 physics goals of the STAR experiment at RHIC in the future.

229 **Acknowledgments**

230 We thank the STAR Collaboration, the RHIC Operations Group and RCF
231 at BNL, and the NERSC Center at LBNL for their support. This work was
232 supported in part by the Offices of NP and HEP within the U.S. DOE Office of
233 Science; Authors Yichun Xu and Zebo Tang are supported in part by NSFC
234 10475071, National Natural Science Foundation of China under Grant No.
235 10610286 (10610285) and Knowledge Innovation Project of Chinese Academy
236 of Sciences under Grant No. KJCX2-YW-A14. One of us (Lijuan Ruan) would
237 like to thank the Battelle Memorial Institute and Stony Brook University for
238 support in the form of the Gertrude and Maurice Goldhaber Distinguished
239 Fellowship.

240 **References**

- 241 [1] J. C. Collins and D. E. Soper, *Ann. Rev. Nucl. Part. Sci.* **37**, 383 (1987);
242 J. C. Collins, D. E. Soper and G. Sterman, *Adv. Ser. Direct. High Energy Phys.*
243 **5**, 1 (1988) [arXiv:hep-ph/0409313]; S. Albino, B. A. Kniehl and G. Kramer,
244 *Nucl. Phys. B* **725** (2005) 181 [arXiv:hep-ph/0502188]; B. A. Kniehl, G. Kramer
245 and B. Potter, *Nucl. Phys. B* **597**, 337 (2001) [arXiv:hep-ph/0011155]; D. de
246 Florian, R. Sassot and M. Stratmann, *Phys. Rev. D* **76**, 074033 (2007)

- 247 [arXiv:0707.1506 [hep-ph]]; S. Albino, B. A. Kniehl and G. Kramer, Nucl. Phys.
248 B **803**, 42 (2008) [arXiv:0803.2768 [hep-ph]].
- 249 [2] L. Ruan [STAR Collaboration], J. Phys. G **34**, S199 (2007)
250 [arXiv:nucl-ex/0701070]; J. Adams *et al.* [STAR Collaboration], Phys. Lett. B
251 **616**, 8 (2005) [arXiv:nucl-ex/0309012]; B. I. Abelev *et al.* [STAR Collaboration],
252 Phys. Lett. B **655**, 104 (2007) [arXiv:nucl-ex/0703040]; J. Adams *et al.* [STAR
253 Collaboration], Phys. Rev. Lett. **97**, 162301 (2006) [arXiv:nucl-ex/0604018].
- 254 [3] J. Adams *et al.* [STAR Collaboration], Phys. Lett. B **637**, 161 (2006)
255 [arXiv:nucl-ex/0601033].
- 256 [4] H. Bichsel, Nucl. Instrum. Meth. A **562** (2006) 154.
- 257 [5] J. Adams *et al.* [STAR Collaboration], Nucl. Phys. A **757**, 102 (2005)
258 [arXiv:nucl-ex/0501009].
- 259 [6] G. Van Buren *et al.*, Nucl. Instrum. Meth. A **566**, 22 (2006)
260 [arXiv:physics/0512157].
- 261 [7] B. I. Abelev *et al.* [STAR Collaboration], Phys. Rev. Lett. **98**, 192301 (2007)
262 [arXiv:nucl-ex/0607012]; J. Adams *et al.* [STAR Collaboration], Phys. Rev.
263 Lett. **94**, 062301 (2005) [arXiv:nucl-ex/0407006]; B. I. Abelev *et al.* [STAR
264 Collaboration], arXiv:0805.0364 [nucl-ex].
- 265 [8] K. H. Ackermann *et al.* [STAR Collaboration], Nucl. Instrum. Meth. A **499**,
266 624 (2003).
- 267 [9] M. Anderson *et al.*, Nucl. Instrum. Meth. A **499**, 679 (2003)
268 [arXiv:nucl-ex/0205014].
- 269 [10] Yan Lu, PH.D. Thesis, Central China Normal University Wuhan, 2005.
- 270 [11] M. Beddo *et al.* [STAR Collaboration], Nucl. Instrum. Meth. A **499** (2003) 725.
- 271 [12] F. S. Bieser *et al.*, Nucl. Instrum. Meth. A **499**, 766 (2003).

- 272 [13] M. Shao, O. Y. Barannikova, X. Dong, Y. Fisyak, L. Ruan, P. Sorensen and
273 Z. Xu, Nucl. Instrum. Meth. A **558**, 419 (2006) [arXiv:nucl-ex/0505026].
- 274 [14] B. I. Abelev *et al.* [STAR Collaboration], Phys. Rev. C **79**, 034909 (2009)
275 [arXiv:0808.2041 [nucl-ex]].
- 276 [15] M. Aguilar-Benitez *et al.*, Z. Phys. C **50**, 405 (1991).
- 277 [16] C. Amsler *et al.* [Particle Data Group], Phys. Lett. B **667**, 1 (2008).

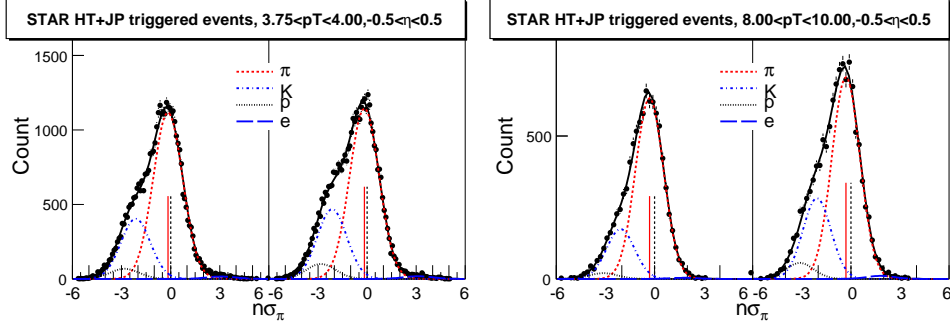


Fig. 1. $n\sigma_\pi^h$ distributions at $3.75 < p_T < 4.0$ GeV/ c and $8.0 < p_T < 10.0$ GeV/ c for the positive (left panel) and negative (right panel) particles. The solid lines are the 8-Gaussian function, which is a sum of the individual Gaussian functions from pion (dashed line), kaon (dot-dashed line), proton (dotted line), and electron (long-dash line). The solid vertical lines are the extracted pion dE/dx positions, while the dashed vertical lines are the previously expected positions.

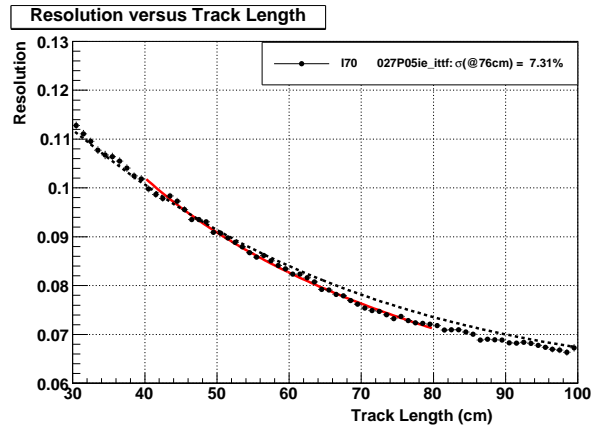


Fig. 2. dE/dx resolution (σ_π) as a function of track length. The red-solid line is a $\sigma_0/t^{0.52}$ power-law fit, and the dashed line is a polynomial function up to 4th power in $\ln(t)$.

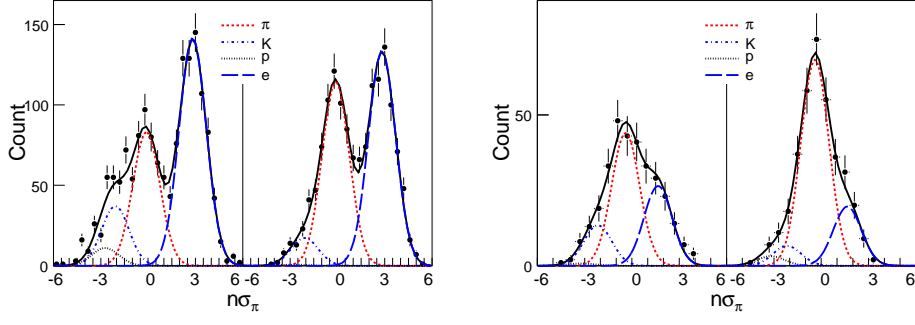


Fig. 3. $n\sigma_\pi^h$ distribution with high-tower trigger at $3.75 < p_T < 4.0$ GeV/c (left panel) and $8.0 < p_T < 10.0$ GeV/c (right panel). Also shown is the result from an 8-Gaussian fit. Both electron and positron yields are enhanced significantly by the trigger.

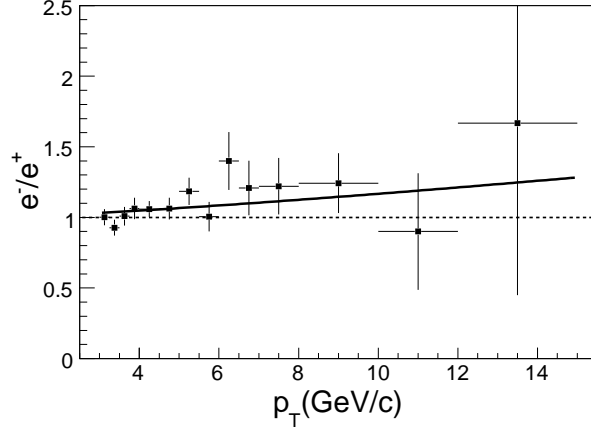


Fig. 4. The ratio of e^-/e^+ as a function of p_T . The curve is a power-law fit described in the text.

Table 1

Fit parameters from momentum and p_T dependence of $n\sigma_\pi^x$ with the function $f(x) = A + \frac{B}{C+x^2}$.

parameters	χ^2/ndf	A	B	C
p dependence	95/49	-0.423 ± 0.015	235 ± 23	464 ± 37
p_T dependence	94/48	-0.443 ± 0.015	234 ± 23	444 ± 35

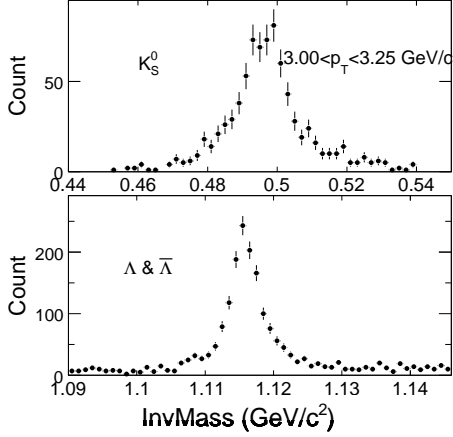


Fig. 5. Invariant mass distributions of K_S^0 (upper panel) and Λ (lower panel) with at least one daughter particle (π or proton) at $3.0 < p_T < 3.25$ GeV/c.

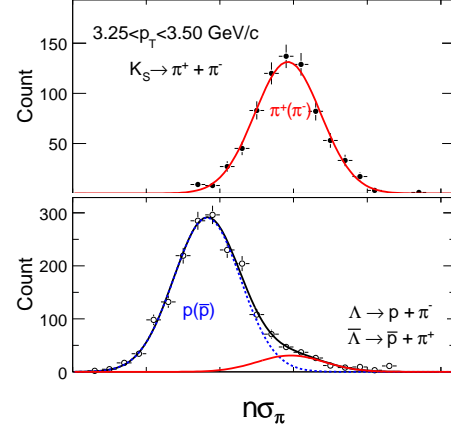


Fig. 6. $n\sigma_\pi^h$ distributions of pions from K_S^0 (upper) and protons (lower) from Λ . The solid line is for pions, and the dashed one for protons.

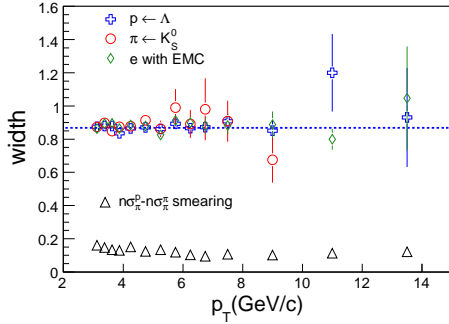


Fig. 7. p_T dependence of dE/dx $n\sigma_\pi^h$ width for proton from Λ decay (crosses), for pion from K_S^0 decay (circles), and for electron enhanced by the EMC (diamond). The open triangle is the smearing positions due to the variation of the track quality (σ_π^p).

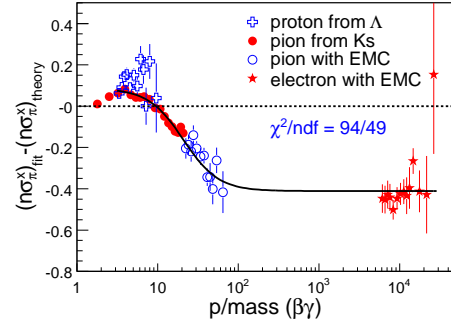


Fig. 8. The dE/dx deviation as a function of $\beta\gamma$. The crosses are for protons from Λ , the filled dots are for pions from K_S^0 , and open circles and stars are for pions and electrons from HT trigger, respectively.

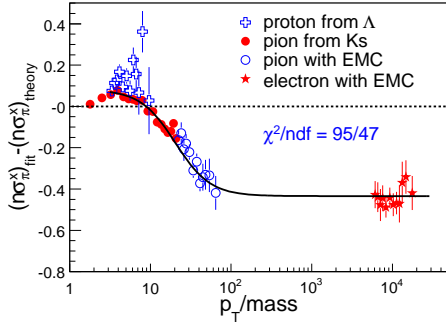


Fig. 9. The dE/dx deviation as function of $p_T/mass$ (similar to Fig. 8).

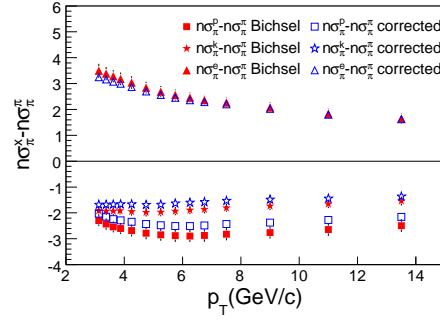


Fig. 10. The relative dE/dx peak positions of $n\sigma_\pi^K$, $n\sigma_\pi^p$, $n\sigma_\pi^e$ as a function of p_T . The solid dots depict theoretical values, and open ones are re-calibrated results.